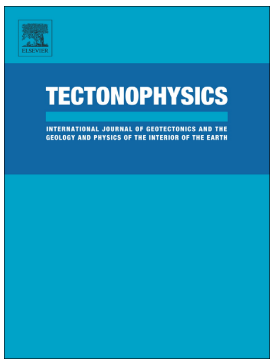

Damage stratigraphy as a controlling mechanism of earthquakes distribution and fault patterns

Zonghu Liao, Lin Zhang, Huayao Zou, Fang Hao, Ze'ev Reches

PII: S0040-1951(22)00455-3

DOI: https://doi.org/10.1016/j.tecto.2022.229661

Reference: TECTO 229661

To appear in: *Tectonophysics*

Received date: 13 March 2022

Revised date: 16 November 2022

Accepted date: 20 November 2022

Please cite this article as: Z. Liao, L. Zhang, H. Zou, et al., Damage stratigraphy as a controlling mechanism of earthquakes distribution and fault patterns, *Tectonophysics* (2022), https://doi.org/10.1016/j.tecto.2022.229661

Damage stratigraphy as a controlling mechanism of earthquakes distribution and fault patterns

Zonghu Liao[1], Lin Zhang[1], Huayao Zou[1], Fang Hao[2], and Ze'ev Reches[3]

[1]State Key Laboratory of Petroleum Resources and Prospecting, China University of Petroleum (Beijing), Beijing 102249, China

[2]School of Geosciences, China University of Petroleum (East China), Qingdao, Shandong 266555, China

[3]School of Geosciences, University of Oklahoma, Norman, OK 73019, USA

Corresponding author: Zonghu Liao (zong@cup.edu.cn)

Abstract

Decollement zones are sub-horizontal weak zones in the earth's crust that strongly affect tectonic deformation. The weakness of a decollement zone is commonly attributed to thermal and composition layering that is relatively static in time. Here, we present evidence for damage stratigraphy in which a stratigraphic unit evolves dynamically into a weak decollement zone. The analysis is focused on the internal structure of a deep, tectonically active, decollement zone in the Sichuan Basin, China. The analyzed zone is about a 1 km thick sequence of Triassic rocks that extends across most of the Sichuan Basin at a depth range of 5.8-6.8 km. This sequence is composed of evaporites (mostly anhydrite) and carbonates (dolomite and limestone). We used three-dimensional seismic surveys, borehole observations, and rock-mechanics experiments to document pervasive internal damage revealed by fractures and flow features within this unit. As this damaged unit is defined by its stratigraphic position, we term it a Damaged Stratigraphic Unit (DSU). The damage-induced weakness of the DSU controls two active tectonic features in the western Sichuan Basin. First, large, intra-basin, frontal thrust faults terminate against the DSU from above and from below. Second, regional earthquakes display a profound decrease in frequency and seismic moment at the depth interval of 5.8-6.8 km that coincides with the DSU. We argue that this earthquake distribution may pose an increased geohazard to the Chengdu area by shallow, moderate earthquakes.

Keywords: Damaged Stratigraphic Unit; Decollement zone; Fault patterns; Earthquakes distribution; Geohazard.

1 Introduction

1.1 Strength of the layered crust

Large-scale strength and rheological variations of the crust are dominated by depth variations of pressure and temperature (Brace & Kohlstedt, 1980; Ranalli & Murphy, 1987). The crust can be divided into two main parts: an upper brittle part, the strength of which is bounded by frictional slip along discontinuities, and a lower ductile part, the strength of which is determined by nonlinear viscoelasticity that depends on temperature, lithology, and strain-rate. It is generally assumed that in tectonically active regions, the in-situ stress depth profile mimics the strength profile, and that the strength profiles can be applied to earthquake distribution (Scholz, 1998; Konstantinou, 2010), the earthquake cycle (Reches et al., 1994), and large scale

decollements associated with plate collisions (Avouac et al., 1993). However, the strength of a rock unit does not necessarily stay constant as the damage processes that are active during tectonic deformation could lead to rock-units weakening causing deformation beyond failure (e.g., Kachanov, 1994; Katz & Reches, 2004; Lyakhovsky & Ben-Zion, 2009; Busetti et al., 2012). The evolving weakening of a stratigraphic unit by ongoing damage is in contrast to relatively static strength associated with thermal, pressure, and lithological properties that were applied by Brace & Kohlstedt (1980).

1.2 Tectonic setting of the present analysis

We analyze the weakening effects of tectonic damage in the Triassic age sequence in the Sichuan Basin, China. The study area is located in the western part of the basin, tens of km east of the seismically active Longmen Shan mountain range (Figure 1a) (Wallis et al., 2003; Burchfiel et al., 2008; Hubbard & Shaw, 2009; Jia et al., 2010; Lu et al., 2019). The Longmen Shan lies to the eastern Tibetan Plateau and defines a marginal topographic transition from the Plateau to Sichuan Basin. It is characterized by four major fault zones: Beichuan (BCF), Pengxian (PXF): Guankou (GKF), and Longquan (LQF) (Fig. 1). Fig. 1 b illustrates the interpreted 3D view of structural architecture for Longmen Shan range and western Sichuan Basin, which is likely formed by a Late Triassic compressional episode and a Cenozoic deformation episode during the India–Asia collision (Burchfiel et al., 2008; Jia et al., 2010; Izquierdo-Llavall et al., 2018; Delcaillau et al., 2022; Qin et al., 2022). Uplift due to crustal shortening resulted in the 2008 Wenchuan earthquake and is continuously activating this region and shaping local topography (Hubbard and Shaw, 2009).

The general stratigraphy of this region consists of a Proterozoic crystalline basement of the Yangtze craton, that is overlain by a sequence of Cambrian dolomites and shales, Permian and Triassic shallow-marine carbonates and evaporites, and Triassic and Jurassic non-marine sandstones and shales (Figure 2) (Jia et al., 2010). Cenozoic tectonism, which is dominated by the India-Asia collision (Burchfiel et al., 2008), generated a series of north-east trending folds and thrusts.

We focus on the internal damage of a ~1 km thick sequence of Triassic carbonates and evaporites at a depth interval of 5.8-6.8 km. The damage of this sequence was directly recognized in borehole logs, core samples, and 3D seismic surveys. We show that this unit serves

as a thick decollement zone that controls the depth distribution of earthquakes and faults. As the damage is bounded to a stratigraphic unit, we refer to it as 'damage stratigraphy', and the present analysis focuses on the *Damaged Stratigraphic Unit* (DSU) of the Triassic sequence in the Sichuan Basin (Figs. 1, 2).

1.3 Methods of subsurface analyses

For the analyses of subsurface damage, we utilized the 3D seismic attribute methodology, including the attributes of amplitude, variance, and curvature (Chopra & Marfurt, 2005) (Supporting Information). It was previously found that subsurface damage is best recognized by the variance attribute that represents the scattering response of acoustic waves by a rock body (Chopra & Marfurt, 2005; Iacopini & Butler, 2011; Liao et al., 2019). High values of the variance attribute indicate intensely damaged and fractured bodies (Iacopini & Butler, 2011), and it was used to map subsurface fault-zones (Liao et al., 2019).

2 Observations: structure, damage, and earthquakes

2.1 Subsurface structure

We investigated the subsurface structure and internal damage of the Triassic sequence DSU by analyzing the three-dimensional seismic surveys within an area of 1,370 km^2 (Fig. 1b); these seismic data are part of the basin-scale petroleum exploration (Lu et al., 2019). The analyzed area is located in the frontal region of the Longmen Shan range, as close as 20 km from the Mw8.0 Wenchuan earthquake hypocenter, and it borders many of the aftershocks of this earthquake (Figure 1a).

The structure of the study area is shown by three subsurface maps (Figures 3a-c) and three complementary vertical seismic profiles (Figure 3d). The maps display the variance and curvature attributes at three depth levels: the Upper Triassic dolomite that is positioned above the damaged strata, the Middle Triassic sequence that we identify as the damage stratigraphic unit (DSU), and the units below the DSU. These maps show consistently higher variance intensity within the DSU (Figure 3b), and along the Pengxian Fault-Zone (PXF in Figure 3). The vertical seismic profiles (Figure 3d) display the DSU at depth of 5.8-6.8 km (light red) where high values of the variance attribute indicate high damage density related to intense fracturing. These apparent displacements of the Pengxian Fault (Figures 3b, d) indicate layer-parallel shear within

the DSU that ranges from ~ 8 km shear at the southwest that gradually decreases and vanishes at the northeast after a horizontal distance of ~50 km. The relatively uniform distribution of the variance attribute within the DSU suggests that the shear was accommodated quasi-uniformly as shown schematically in Figure 3e.

The Pengxian Fault, which is the dominant fault in the study area (PXF in Figures 1b, 3), is regarded as a frontal blind thrust that propagated from the Longmen Shan range (Lu et al., 2019). The Pengxian Fault displays some striking relationships with the DSU. First, this fault is terminated and displaced by the DSU (red arrows in Figure 3d): In the southwest profile (left profile, Figure 3d), the upper segment of the Pengxian Fault is displaced eastward by about 8 km relative to the lower segment, in the middle profile, the fault is displaced by only ~2 km, and in the northeast profile (right profile, Figure 3d), the Pengxian Fault is not displaced. Further, at the northeast profile, the DSU displays noticeable thickening at the intersection with the Pengxian Fault. Second, the damage zones of the Pengxian Fault reveal contrasting structures above and below the DSU. Above the DSU (Figure 3a), the Pengxian Fault appears as a relatively linear zone that extends for 55 km via a fold-fault system. Below the DSU (Figure 3c), the fault zone is bent and twisted with curved subsidiary segments, and it extends for a greater length than above the DSU. We deduce that the presence of the DSU led to the separation of the Pengxian Fault into these two contrasting structural styles; the controlling mechanism will be discussed later.

2.2 Depth distribution of subsurface damage

Above, we presented maps and profiles of the variance attribute as an indicator of subsurface damage intensity (Figure 3). We now examine the depth distribution of this variance. The seismic profile (Figure 4a) and the attribute depth profile (Figure 4b) reveal three zones of high damage intensity: 1. A shallow damage zone at < 3 km depth, with the most-high variance values of 0.3-0.5. We relate this damage to intense brittle fracturing under the relatively low confining pressure; 2. The zone at 5.8-6.8 km depth of variance of 0.1-0.2 of the Triassic DSU described above. The mechanisms of the brittle-ductile damage are associated with the lithology in this stratigraphic unit as discussed later; and 3. A zone at 8-10 km depth with a variance of 0.1-0.2. We relate this damage to deformation localized at the contact between the sedimentary sequence and the crystalline basement.

2.3 Regional seismic activity

The study area is located at the margins of the Longmen Shan range, close to the hypocenter of the 2008 Mw8.0 Wenchuan earthquake. To explore the effects of a ~ 1 km thick DSU on the regional seismic activity, we examined the catalog of more than 40,000 earthquakes in the upper crust (depth <25 km) for this area during the 2008-2012 period. The spatial distribution of the epicenters is displayed in Figure 1b, and their depth distribution is displayed on a tectonic cross-section across with earthquake hypocenters projected to the section (Figure 4c). The depth distribution of the cumulative seismic moments was calculated in depth intervals of 0.1 km, which is the depth resolution of the earthquakes in the catalog, and the smoothen data in 0.5 km depth intervals are displayed in Figure 4d.

The outstanding feature in Figure 4 is the correlation of the depth distribution of the earthquake cumulative moments (Figure 4d) with the damage zone as observed in Figure 3 and Figure 4b. This correlation is noted by the decrease of earthquake moment at hypocenter depths of 4–8 km which correlates with the 5.8-6.8 depth of the damaged stratigraphic unit. We argue below that this decrease of seismic activity surrounding DSU can be attributed to the relaxation of tectonic loading by the weak DSU.

3 Analysis: Rheology and strength of the DSU in the Sichuan Basin

The above descriptions indicate that the Triassic sequence (DSU) in the western Sichuan Basin is pervasively damaged, and that its presence affects the fault pattern (Figure 3) and earthquake distribution (Figure 4). We now analyze possible mechanisms for these observations.

The lithological composition of the DSU in the study area was documented in the LS1 borehole that was drilled to a depth of 7,100 m (location in Figures 1b, 4a, c). The borehole logs (Figure 2) indicate that the 5.8-6.8 km depth interval includes ~400 m of anhydrite, ~200 m anhydrite mixed with dolomite breccia, and ~600 m of fractured dolomites and limestones. Rock samples collected during drilling provide direct evidence of pervasive damage within the DSU (Figures 5, 6). These samples reveal cataclasis at scales of centimeter to decimeter of the brittle dolomite samples, and at the millimeter scale in thin sections. For example, Figure 5 shows fractures in the matrix of the dolomite that are filled with anhydrite that display a similar style to the experimental fracturing of a dolomite core embedded inside ductile limestone (Figure 5e). The thin-sections display abundant elongated anhydrite crystal grains that surround the dolomite

fragments (Figure 6). The brittle dolomite blocks rotated within the ductile anhydrite zones, that together composed brittle-ductile deformation within the DSU.

3.1 Strength and ductility of Triassic rocks in Sichuan Basin

We envision that the evaporite/carbonate composition of the Middle and Upper Triassic in the Sichuan Basin controls the rheology and strength by integration of thermally controlled ductility of the anhydrite and damage cataclastic flow of the brittle carbonates. We evaluate the strength of the DSU in three steps: experimental tests of samples within the DSU, thermal ductility of anhydrite, and evaluation of damage weakening. Recently, the mechanical properties of Triassic rocks from the Sichuan Basin were analyzed in rock-mechanics experiments (Supporting Information). The tested samples, which belong to the same stratigraphic unit of the DSU, were collected at a depth range of 4.7-4.8 km in oil production wells located ~100 km away from our study area (Figure 2) (Kibikas, 2021).

We present the experimental results of three samples that represent the lithology range of the DSU (Figure 7): pure anhydrite (sample EV1), calcitic dolomite (sample DS1), and dolomitic-limestone (sample LS2) (Kibikas, 2021). The triaxial testing was conducted on water-saturated samples that were loaded to failure and beyond under 22.5 MPa confining pressure and temperatures of 23°C and 50°C. The samples reached the ultimate strength at an axial strain of 0.5-0.7%. The stress-strain data of these experiments show that the anhydrite (EV1) deformed in a ductile style even at room temperature with only gentle strength reduction with increasing strain (Figure 7). The carbonate samples (LS2 and DS1) failed in a brittle-ductile style at both temperatures, but continued to flow in a quasi-ductile style after axial strain > 1% under approximately constant differential stress of ~130 MPa (LS1) and ~160 MPa (DS1). We envision that under in-situ conditions of 5.8-6.8 km depth of the DSU will flow at even lower differential stresses.

3.2 Thermally controlled ductility

The large-scale strength of the crust is evaluated for a brittle upper part, in which the strength is bounded by frictional slip, and a ductile lower part, in which the strength is controlled by viscoelasticity (Brace & Kohlstedt, 1980). We apply this approach to the study area by assuming that the DSU strength is governed by the flow of its anhydrite component. We used the

experimental analysis of Moller & Briegel (1978) who tested Riburg anhydrite samples from a borehole in the Jura tectonic region, Switzerland. These samples were deformed at 150 MPa confining pressure, temperatures up to 450°C, and strain-rates as low as 10^{-7} s^{-1}. Moller & Briegel (1978) found that at a temperature of ~200°C and under a tectonic strain-rate of 10^{-14} s^{-1}, which are the approximate conditions at the DSU depth, the tested anhydrite is stronger than halite and weaker than Solenhofen limestone (Figure 7 of Moller & Briegel, 1978). We regard these experimental results as a suitable representative of the pure anhydrite layers in the Sichuan Basin. The strength profile for the Sichuan Basin was calculated (Supporting Information) by application of anhydrite rheology to the rock sequence at the DSU depth (Figure 8a). The profile indicates that the shear strength of this unit is 30-60% of the strength of the layers above and below it.

3.3 Damage induced weakening

Experimental analyses revealed that brittle rocks subjected to elevated confining pressure are continuously damaged by microfracturing from loading initiation to failure and beyond (e.g., Griggs and Handin, 1960; Lockner et al., 1991). The microfracturing damage leads to global weakening and reduction of Young modulus, as demonstrated in experiments (Lockner et al., 1991; Katz & Reches, 2004), predicted in theoretical modeling (Kachanov, 1994; Lyakhovsky & Ben-Zion, 2009), and simulated in numerical calculations (Busetti et al, 2012) (Figure 7b). These analyses indicate that after failure, damaged brittle rocks may continuously deform by cataclastic flow under a quasi-constant, lower differential stress (Figure 7b) (Wong et al., 1997; Vajdova et al., 2010; Busetti et al., 2012).

Further, the deformation style of a heterogeneous/composite rock would be even more susceptible to damage creep. These rocks are composed of mixed brittle component of dolomite/limestone and ductile component of anhydrite (Figs. 5, 6; Griggs and Handin, 1960). In this case, the deformation is distributed (Fig, 5e) while each component deforms in each own style. The global, macroscopic stress-strain curve display creeping behavior after the initial strain hardening stage (Fig. 1 in Griggs and Handing, 1960; some of our samples in Fig. 7). We thus argue that the pervasive damage within the Triassic units of Sichuan Basin leads to creeping without major localization, and by doing so relaxes the tectonic loading above and below the DSU.

We argued in the Introduction that the damage rheology and the associated deformation evolve penecontemporaneously during the tectonic loading phase. This strength evolution differs from the strength that depends on rock type and loading conditions that are quasi-stable in time, e.g., the lower crust. This argument is based on experimental results and modeling of damage rheology (e.g., Kachanov, 1994; Katz & Reches, 2004; Lyakhovsky & Ben-Zion, 2009; Busetti et al., 2012), however, the observations in the present study area do not provide information on the time and rate of the damage weakening processes.

4. Discussion: Damage stratigraphy and earthquakes distribution

4.1 DSU control of fault patterns

The pervasive damage in the DSU (Figures 3, 4b), the evaporite flow (Figure 5), and rock-mechanics observations (Figure 7), all indicate that the Middle-Upper Triassic sequence in the Sichuan Basin is relatively weak. This weakness evolved by a combination of ductile flow of the evaporite layers coupled with the cataclastic flow of the damaged brittle carbonates. This ~1 km thick DSU has the suitable properties to become a decollement zone: relative weakness (Figures 8a, 9a), sub-horizontal position, and regional extent across the entire Sichuan Basin. The effects of this Triassic decollement are first examined with respect to the termination and shifting of crustal-scale faults (Figures 3d, 4a).

It was shown above that the Pengxian Fault terminates toward the DSU and is shifted by it (Figures 3d, 4a). In a brittle medium, the front zone of a fault is characterized by intense stress amplification that facilitates fault propagation (e.g., Reches and Lockner, 1994). However, the inverse is expected as a fault approaches a weak region in which the failure/flow relaxes and diffuses the stress amplification. As a result, the fault propagation as a distinct discontinuity is blunted, and the localized shear is converted to distributed deformation. For example, experimental simulations with viscous layering as an evaporite analogue revealed blunting of brittle faults (Brun et al., 1994; Koyi & Skelton, 2001). Similarly, the blunting of fault propagation by a ductile layer was documented in rifting off-shore Norway where salt layers of Middle-Upper Triassic disconnected faults in the brittle layers above or below. We envision that the thick, weak-ductile layers of the present DSU, act as agents of rupture blunting (Begley et al., 1977) that leads to a wide deformation zone (Figure 3d), and prevents fault propagation across it.

4.2 DSU control of earthquake distribution

Distinct reduction of earthquake occurrence with depth (Figure 3c) was observed at the proximity of weak, ductile/viscous zones elsewhere (e.g., Bonner et al., 2003). For example, Sibson (1982) reviewed the depth distribution of earthquakes in the continental US, and concluded that "…the depth of seismic activity is controlled by the passage from a pressure-sensitive, dominantly frictional regime to strongly temperature-dependent, quasi-plastic mylonitization at greenschist and higher grades…". Konstantinou (2010) analyzed the relationships between crustal strength, earthquake distribution, and the 1956 Amorgos earthquake in the southern Aegean region (Figure 8c). Their heat flow and lithology calculations revealed that the interval of 7-15 km depth has the lowest effective viscosity, namely the weakest layer, in the upper 30 km of the crust (red curve in Figure 8c). Konstantinou (2010) further showed that the depth distribution of 142 relocated earthquakes in these regions displays a profound reduction at the lower-crust depth (bars in Figure 8c). Similarly, we attribute the reduction of earthquake occurrence in our analysis (Figures 4d, 8b) to the damage-controlled weakness that relaxes the buildup of in-situ stresses during interseismic periods by continuous damage and cataclastic flow.

4.3 Potential DSU effect on geohazard

Our analysis also reveals a profound increase of the occurrence of earthquakes in the upper two kilometers of the study area (blue arrow in Figure 4d). This observation may pose increased geohazard to the Chengdu region. The regional geohazard estimations focused on the moderate-to-large earthquakes of the Longmen Shan range (Wallis et al., 2003; Burchfiel et al., 2008; Hubbard et al., 2010; Jia et al., 2010; Lu et al., 2019). However, small-to-moderate magnitude earthquakes that occur at shallow depth and in the near-field can pose a major local hazard. Bommer et al. (2001) described a few cases of moderate earthquakes with a catastrophic outcome, and stated: "…there have been many cases where earthquakes of moderate and even small magnitude have caused very significant destruction when they have coincided with population centers. Even though the area of intense ground shaking caused by such events is generally small, the epicentral motions can be severe enough to cause damage even in well-engineered structures." Further, Bommer et al. (2001), emphasized the combined effect of epicenter distance and earthquakes depth, for example, the predicted peak ground acceleration

for a M5.5 earthquake at 1 km epicenter distance and 20 km depth is 0.1g, but the same event at 2 km depth could generate ~1g of peak acceleration (Figure 8d). Based on our observations (Figures 4c-d) and the analysis of Bommer et al. (2001), we argue that the Chengdu area may suffer significant ground motion during small-to-moderate shallow earthquakes (Figure 9b) if they occur in the near-field.

4 Conclusions

The present analysis demonstrates that the pervasive damage and flow within a thick stratigraphic unit would generate a weakened zone during tectonic deformation. This unit will serve as a perfect, thick decollement zone within the upper crust that controls the style of faulting and earthquake distribution. While our investigation focused on the western Sichuan Basin, the "localized" lithological characteristics on the studied Triassic unit are common in sedimentary basins, and we argue that similar damage decollement zones are active elsewhere.

Acknowledgments, Samples, and Data

We thank Samuel Angiboust, An Yin, and three other anonymous reviewers for their insightful comments. We thank Brett M. Carpenter, University of Oklahoma, for the useful discussions. We acknowledge Sinopec for providing drilling cores and three-dimensional seismic survey used in this study, Lihua Fang for providing his seismic catalog, and William Kibikas for providing the data of his experimental analysis. Support funds were provided by National Key Research and Development Program of China 2019YFC0605502, Chinese Academy of Sciences SPRP XDA14010306, and ISE-NSFC Joint Scientific Research Program 42161144005. The authors declare no financial or other conflicts of interest.

Data Availability Statement

The strength calculation of the sediment lithology in Sichuan Basin, the original and analyzed seismic data, and Tri-axial experimental results of the carbonate and evaporate are uploaded to Zenodo and are freely available through the DOI link (http://doi.org/10.5281/zenodo.4596081).

References

Avouac, J.-P., P. Tapponnier, M. Bai, H. You, & G. Wang (1993). Active thrusting and folding along the northern Tien-Shan and Late Cenozoic rotation of the Tarim relative to Dzungaria and Kazakhstan. J. Geophys. Res., 98(B4), 6755-6804.

Bommer, J. J., Georgallides, G., and Tromans, I. J. (2001). Is there a near-field for small-to-moderate magnitude earthquakes? Bull. Earthquake Eng., 5, 395-423.

Bonner, J. L., Blackwell, D. D., & Herrin, E. T. (2003). Thermal constraints on earthquake depths in California. Bull. Seis. Soc. Am., 93, 2333-2354.

Byerlee, J. (1978). Friction of rocks. Rock friction and earthquake prediction Birkhäuser, Basel, p. 615-626.

Brace, W. F., & Kohlstedt, D.L. (1980). Limits on lithospheric stress imposed by laboratory experiments. J. Geophys. Res., 85, 6248-6252.

Busetti, S., Mish, K., & Reches, Z. (2012). Damage and plastic deformation of reservoir rocks: Part 1. Damage fracturing. AAPG Bull. 96, 1687-1709.

Begley, J. A., Logsdon, W. A., & Landes, J. D. (1977). Ductile rupture blunt-notch fracture criterion. In Flaw Growth and Fracture. ASTM Int.

Burchfiel, B. C., Royden, L. H., Van der Hilst, R. D., & Hager, B. H. (2008). A geological and geophysical context for the Wenchuan earthquake of 12 May 2008, Sichuan, PRC. GSA Today, 18, 4-11.

Brun, J. P., Sokoutis, D., & Van Den Driessche, J. (1994). Analogue modeling of detachment fault systems and core complexes. Geology, 22, 319-322.

Chopra, S., & Marfurt, K. J. (2005). Seismic attributes-A historical perspective. Geophysics, 70, 3SO-28SO.

Delcaillau, B., Graveleau, F., Saint Carlier, D., Rao, G., Le Béon, M., Charreau, J., & Nexer, M. (2022) Geomorphic analysis of active fold growth and landscape evolution in the central Qiulitage fold belt, southern Tian Shan, China, Geomorphology, 398, 108063.

Fang, L., Wu, j., Wang, W., Du, W., Su, J., Wang, C., Yang, T., and Cai, Y. (2015). Aftershock observation and analysis of the 2013 M S 7.0 Lushan earthquake. Seis. Res. Lett., 86, 1135-1142.

Griggs, D., and Handin, J. (1960). Observations on fracture and a hypothesis of earthquakes. in Griggs and Handin, editors, "Rock Deformation" GSA Memoir 79, Ch. 13.

Hubbard, J., & Shaw, J. H. (2009). Uplift of the LMS and Tibetan Plateau, and the 2008 Wenchuan (M=7.9) earthquake. Nature, 458, 194-197.

Hubbard, J., Shaw, J. H., & Klinger, Y. (2010). Structural setting of the 2008 M w 7.9 Wenchuan, China, earthquake. Bull. Seism. Soc. Am., 100, 2713-2735.

Iacopini, D., & Butler, R. W. (2011). Imaging deformation in submarine thrust belts using seismic attributes. Earth Planet. Sci. Lett., 302, 414-422.

Izquierdo-Llavall, E., Roca, E., Xie, H., Pla, O., Muñoz, J. A., Rowan, M. G., ... & Huang, S. (2018). Influence of overlapping décollements, syntectonic sedimentation, and structural inheritance in the evolution of a contractional system: The central Kuqa fold-and-thrust belt (Tian Shan Mountains, NW China). Tectonics, 37(8), 2608-2632.

Jia, D., Li, Y., Lin, A., Wang, M., Chen, W., Wu, X., Ren, Z., Zhao, Y., & Luo, Y. (2010). Structural model of 2008 Mw 7.9 Wenchuan earthquake in the rejuvenated Longmen Shan thrust belt, China. Tectonophysics, 491, 174-184.

Kachanov, M. (1994). On the concept of damage in creep and in the brittle-elastic range. Int. J. Damage Mech., 3, 329-337.

Katz, O., & Reches, Z. (2004). Microfracturing, damage, and failure of brittle granites. J. Geophys. Res., 109.

Kibikas, W. (2021). Characterizing Rock Properties and their Impact on the Mechanical Behavior of Crystalline Basement and Caprocks (Doctoral dissertation, University of Oklahoma).

Konstantinou, K. I. (2010). Crustal rheology of the Santorini-Amorgos zone: Implications for the nucleation depth and rupture extent of the 9 July 1956 Amorgos earthquake, southern Aegean. J. Geodynamics, 50, 400-409.

Koyi, H. A., & Skelton, A. (2001). Centrifuge modelling of the evolution of low-angle decollement faults from high-angle normal faults. J. Struct. Geol., 23, 1179-1185.

Lyakhovsky, V., & Ben-Zion, Y. (2009). Evolving geometrical and material properties of fault zones in a damage rheology model. Geochemistry, Geophysics, Geosystems, 10, 11.

Lockner, D., Byerlee, J. D., Kuksenko, V., Ponomarev, A., & Sidorin, A. (1991). Quasi-static fault growth and shear fracture energy in granite. Nature, 350, 39-42.

Lu, R., He, D., Xu, X., Tan, X., Li, Y., Cai, M., & Wang, Z. (2019). Geometry and kinematics of buried structures in the piedmont of the central Longmen Shan: implication for the growth of the Eastern Tibetan Plateau. J. Geol. Soc. London, 176, 323-333.

Liao, Z., Liu, H., Carpenter, B. M., Marfurt, K. J., & Reches, Z. (2019). Analysis of fault damage zones using three-dimensional seismic coherence in the Anadarko Basin, Oklahoma. AAPG Bull., 103, 1771-1785.

Moller, W.H., & Briegel, U. (1978). The rheological behavior of polycrystalline anhydrite. Eclogae Geol. Helv., 71, 397-407.

Peng, S., & Johnson, A. M. (1972). Crack growth and faulting in cylindrical specimens of Chelmsford granite. In Int. J. Rock Mech. Min. Sci & Geomech. Abstracts, 9, 37-86.

Qin, X., Chen, X., Shao, Z., Zhang, Y., Wang, Y., & Li, B. (2022). Cenozoic multi-phase intracontinental deformation of the Tianshan Range (NW China): Constraints from detrital zircon provenance and syn-tectonic sedimentation of the Kuqa Depression, Journal of Asian Earth Sciences, 232, 105183.

Reches, Z., & Lockner, D. A. (1994). Nucleation and growth of faults in brittle rocks. J. Geophys. Res., 99(B9), 18159-18173.

Ranalli, G., & Murphy D. C. (1987). Rheological stratification of the lithosphere. Tectonophysics, 132, 281-295.

Reches, Z. E., Schubert, G., & Anderson, C. (1994). Modeling of periodic great earthquakes on the San Andreas fault: Effects of nonlinear crustal rheology. Journal of Geophysical Research: Solid Earth, 99(B11), 21983-22000.

Scholz, C. H. (1998). Earthquakes and friction laws. Nature, 391, 37-42.

Sibson, R. H. (1982). Fault zone models, heat flow, and the depth distribution of earthquakes in the continental crust of the United States. Bull. Seis. Soc. Am., 72, 151-163.

Vajdova, V., Zhu, W., Chen, T. M. N., & Wong, T. F. (2010). Micromechanics of brittle faulting and cataclastic flow in Tavel limestone. J. Struct. Geol., 32, 1158-1169.

Wallis, S., Tsujimori, T., Aoya, M., Kawakami, T., Terada, K., Suzuki, K., & Hyodo, H. (2003), Cenozoic and Mesozoic metamorphism in the Longmenshan orogeny: Implications for geodynamic models of eastern Tibet. Geology, 31, 745-748.

Wong, T. F., David, C., & Zhu, W. (1997). The transition from brittle faulting to cataclastic flow in porous sandstones: Mechanical deformation. J. Geophys. Res., 102, 3009-3025.

Zhang, Y., Dong, S., and Yang, N. (2009). Active faulting pattern, present-day tectonic stress field and block kinematics in the east Tibetan Plateau. Acta Geolog. Sinica, 83, 694-712.

Figure captions

Figure 1. Tectonic setting of the study area adjacent to the Longmen Shan range and Tibetan Plateau. **(a)** Left: General location with inset of the study region. Right: Tectonic map of western Sichuan Basin that displays: (1) Region of the analyzed seismic survey covering 1370 km^2 (blue polygon close to the southwest corner); (2) Earthquakes epicenters for 2008-2012 period, including the 2008 Wenchuan Mw=8.0 earthquake, and the 2015 Mw=6.7 Lushan earthquake; (3) Site of the LS1 well; and (4) The major fault zones, Beichuan (BCF), Pengxian (PXF): Guankou (GKF), and Longquan (LQF). **(b)** Interpreted 3D view of structural architecture for the Longmen Shan range and western Sichuan Basin (after Zhang et al., 2009), including the hypocenter of the 2018 Wenchuan earthquake and the analyzed Triassic damage unit (light red).

Figure 2. Stratigraphic section of the Triassic damage unit at a depth interval of 5.8-7 km as determined in Longshen 1 borehole. The unit's lithology is dominated by anhydrite (red), dolomite, and limestone, and core images appear in the right column. Close-up of selected core images are displayed in Fig. 5.

Figure 3. Horizontal and vertical sections of the damage-stratigraphic-unit (DSU) that are displayed by the seismic attribute of variance co-rendered with curvatures recognized in the three-dimensional seismic survey (Methods, Supporting material). **(a)** Horizontal section of the

dolomite layers above the DSU. Note the linear trend of the Pengxian Fault (PXF). **(b)** The horizontal section within the DSU with thickness contours (yellow dashed curves). The red arrows indicate the displacement of the Pengxian Fault by the DSU as recognized by comparing PXF positions in **(a)** and **(c)** (text). **(c)** Horizontal section of dolomite and limestone layers below the DSU. **(d)** Vertical seismic sections across the DSU; the location of each section is marked by a green line at the lower inserts; the sections display the amplitude attribute co-rendered with variance attribute, and the Pengxian Fault (black lines). **(e)** A schematic presentation of the apparent displacement of the PXF by ~8km within the DSU as interpreted in (d). Note the DSU (red), and the red arrows indicating the displacement direction of the PXF by the DSU.

Figure 4. Damage stratigraphy, fault patterns, and earthquake distributions. **(a)** An extended vertical seismic section in NW-SE direction (green line A-A' in Figure 1a); It displays amplitude co-rendered with variance attribute. The section displays the DSU (transparent red) and fault systems (black lines). Horizontal scale: vertical scale=1:2. **(b)** Depth profile of the average values of seismic variance for the stratum surrounding the Pengxian Fault, but excluding the fault damage zones. Note three zones of higher variance values that correspond to intense damage (text). **(c)** Interpreted geological cross-section of (4**a**), with projected hypocenters of the seismic events. **(d)** Depth profile of cumulative moments of the earthquakes of the 2008-2012 period (4c) calculated at 0.25 km depth intervals. Note a relative increase of cumulative seismic moment at shallow depth (blue arrow) and a relative decrease of the cumulative seismic moment at 5-8 km depth of the DSU (text).

Figure 5. (**a-d)** Images of core samples collected at Longshen 1 borehole (Figures 1a, 2) displaying centimeter-scale flow of anhydrite (bright zones) that fills the spaces between fractured and fragmented dolomite (dark gray). **(e)** Cross-section of an experimental sample deformed under high confining pressure that displays a core of fractured brittle dolomite embedded within ductile limestone (Griggs and Handin, 1960).

Figure 6. Photomicrographs of thin-sections of core samples from the damage unit displaying anhydrite and dolomite relationships; sample collection depth in the upper right. (**a-c)** plane-light views of dolomite fragments (black) floating in anhydrite (dark gray). (**d-f)** cross-polarized views of (**a-c)**; note elongated anhydrite grains in **d**.

Figure 7. Stress-strain relationships in rock-mechanics experiments of anhydrite and carbonates samples. **a**, Differential stress (axial stress – confining pressure) as a function of the

axial strain of three rock types from the Triassic damage unit in the Sichuan Basin; composition and experimental details appear in the text, after Kibikas (2021). The plot shows the results of saturated samples at 22.5 MPa effective confining pressure that were loaded to failure and beyond at temperatures of 23 °C and 50 °C. **b**, Differential stress curves of three experiments of Berea sandstone loaded at three confining pressures (solid curves); the numerically simulated damage intensity for each test is marked by dashed curves. Modified after Fig. 6 of Busetti et al., (2012).

Figure 8. Crustal strength and earthquake depth distribution. (**a**) The crust strength in the Sichuan Basin are calculated to two rheological components: frictional strength of the brittle part following Byerlee law, and ductile strength of the evaporite-carbonate sequence by using the experimental rheological results of anhydrite (text and Supporting Information). (**b**) Depth profile of cumulative moments of the earthquakes of the 2006-2012 period calculated at 0.25 km depth intervals (same as Fig. 4d, text). (**c**) The relationships between the crustal strength, shown by effective viscosity (red curve), and depth distribution of 142 earthquakes (gray columns) in the southern Aegean region (modified after Konstantinou [2010], see text). Note the positive correlation between the strength reduction and reduction of earthquake occurrence in the 12-16 km depth. (**d**) Expected intensity of peak horizontal acceleration for a moderate earthquake (Mw=5.5) for the displayed range of hypocentral depths and distance from the earthquake epicenter (after Bommer et al., 2001).

Figure 9. Schematic model of crustal strength and earthquake depth distribution. **(a)** Schematic strength profile for sedimentary sequences with a weak, damaged unit. **(b)** Expected earthquake depth distribution in the presence of a weak zone due to damage-induced thermal control or lithology (see text and Figure 8; the right one is for comparison).

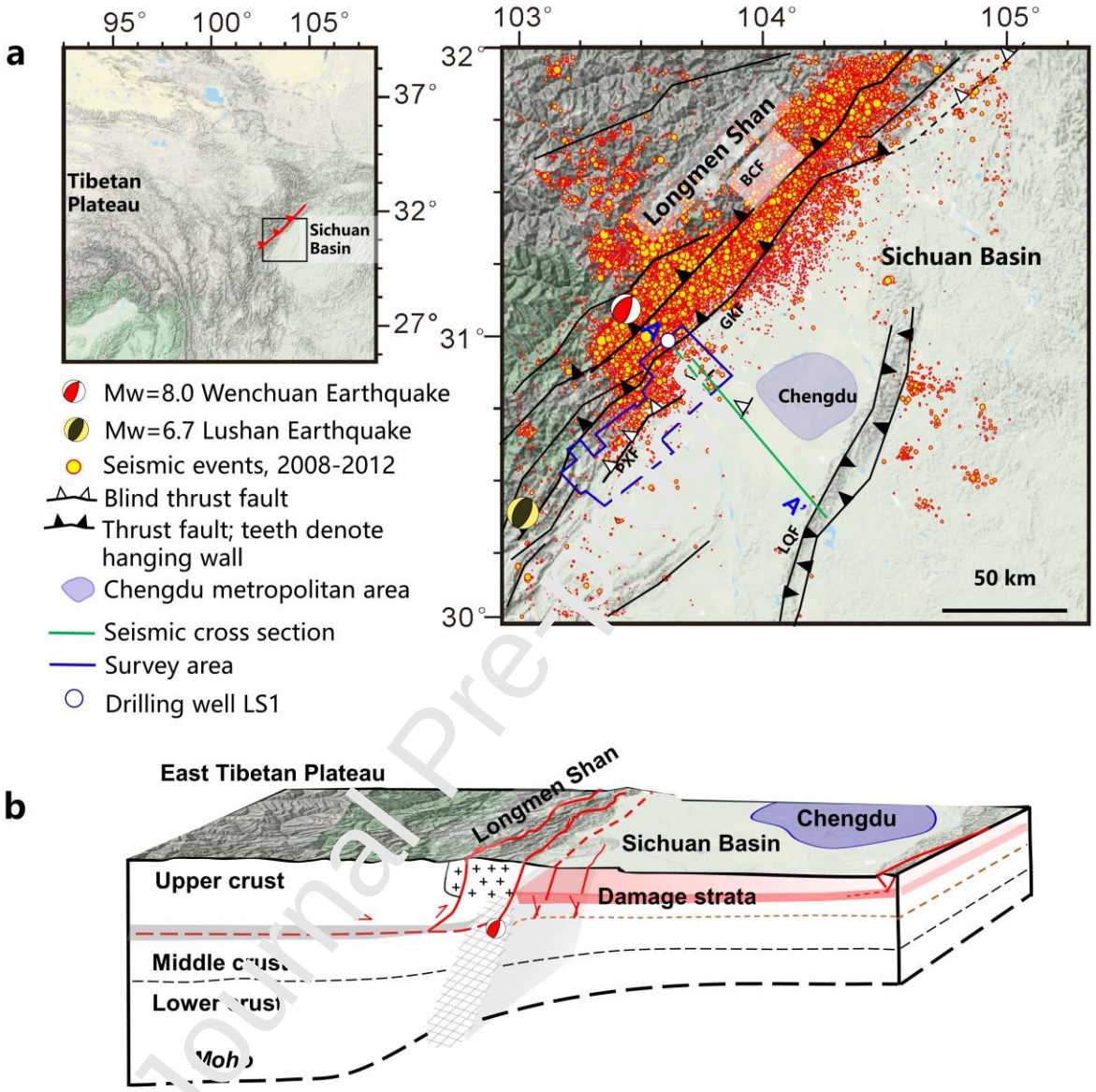

Fig. 1

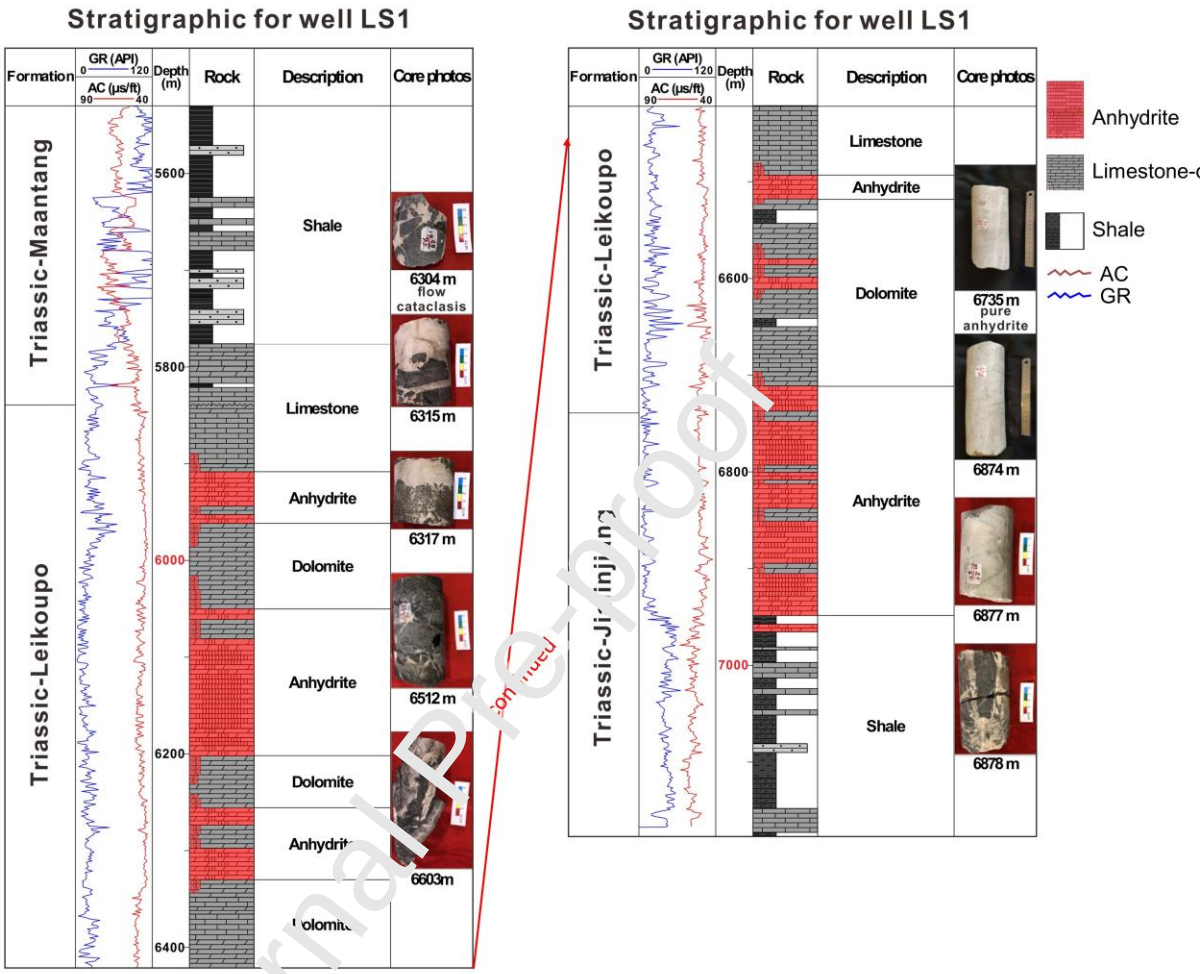

Fig. 2

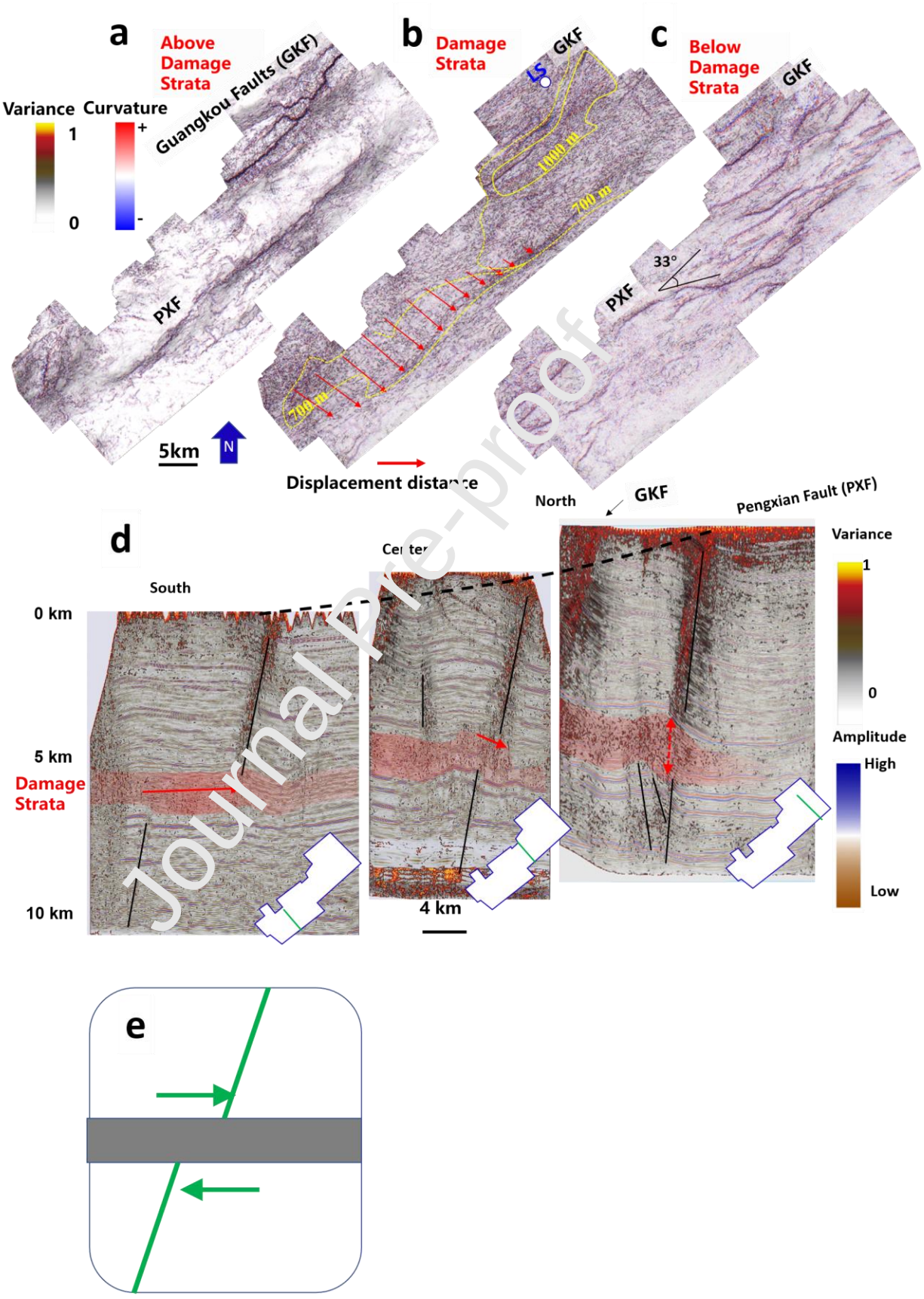

Fig. 3

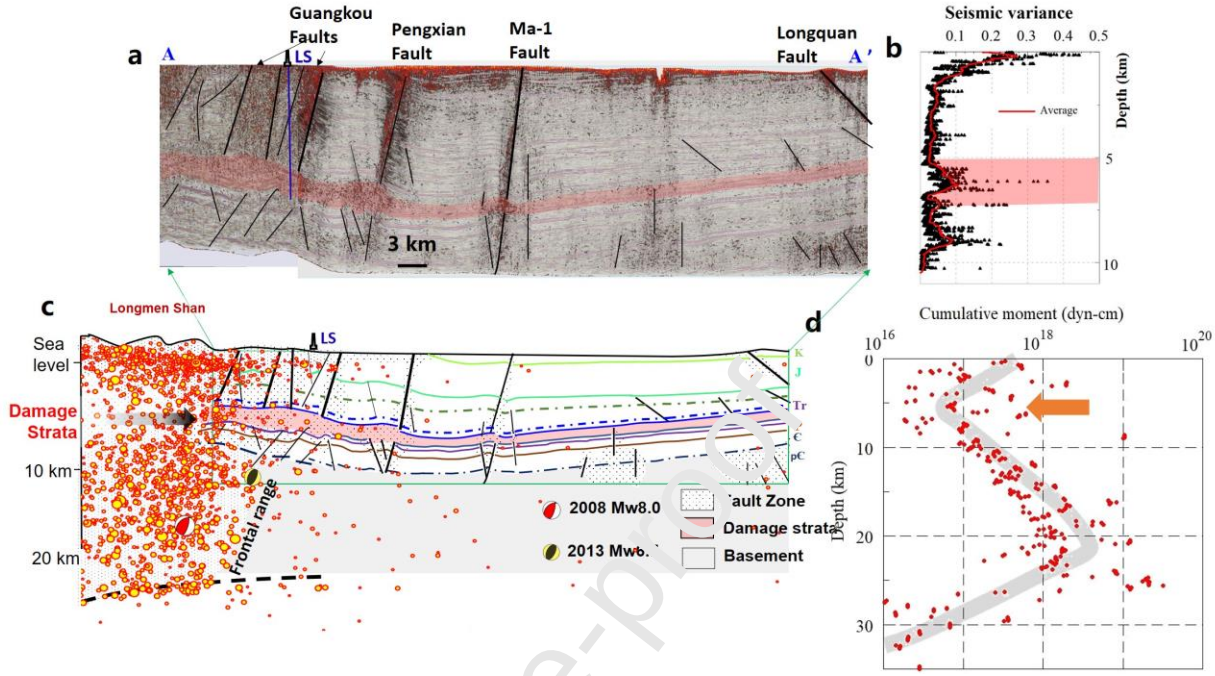

Fig. 4

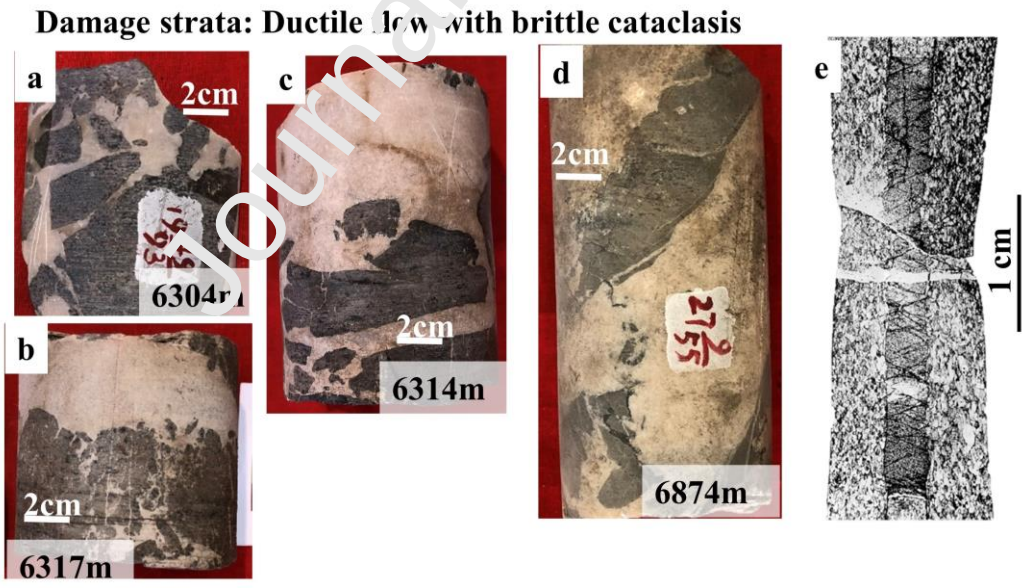

Fig. 5

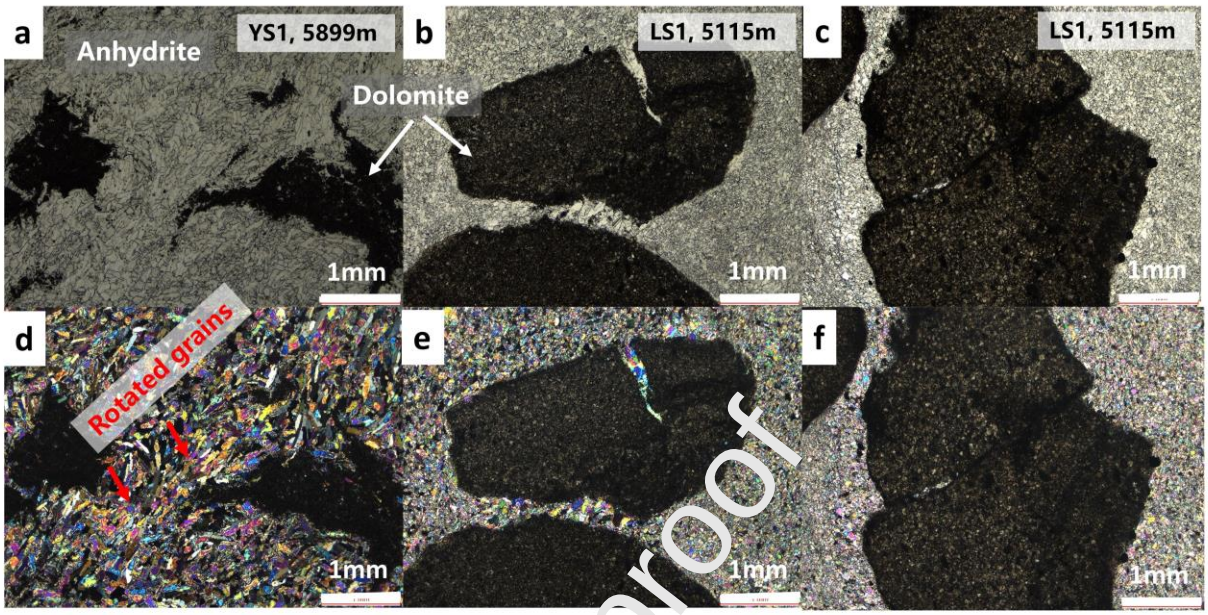

Fig. 6

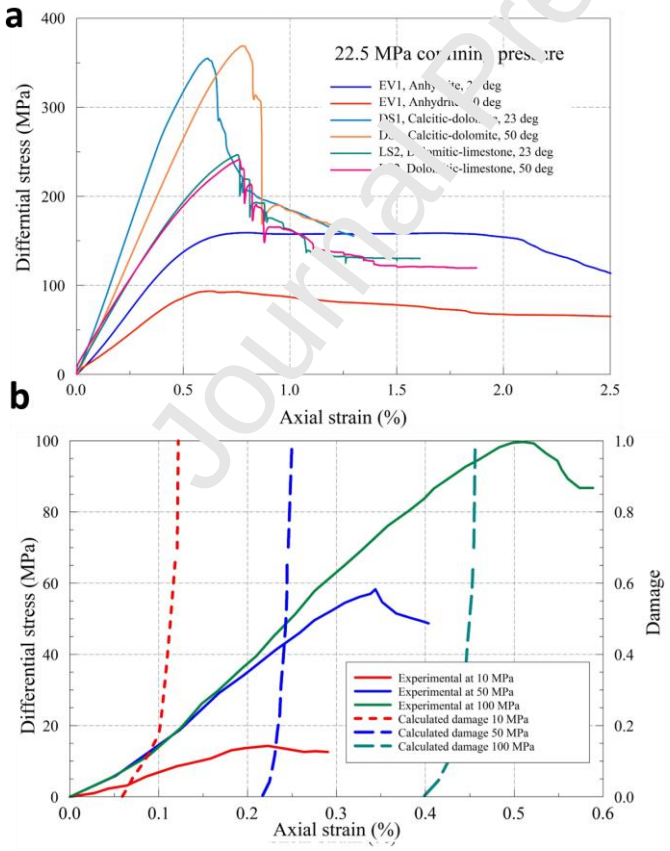

Fig. 7

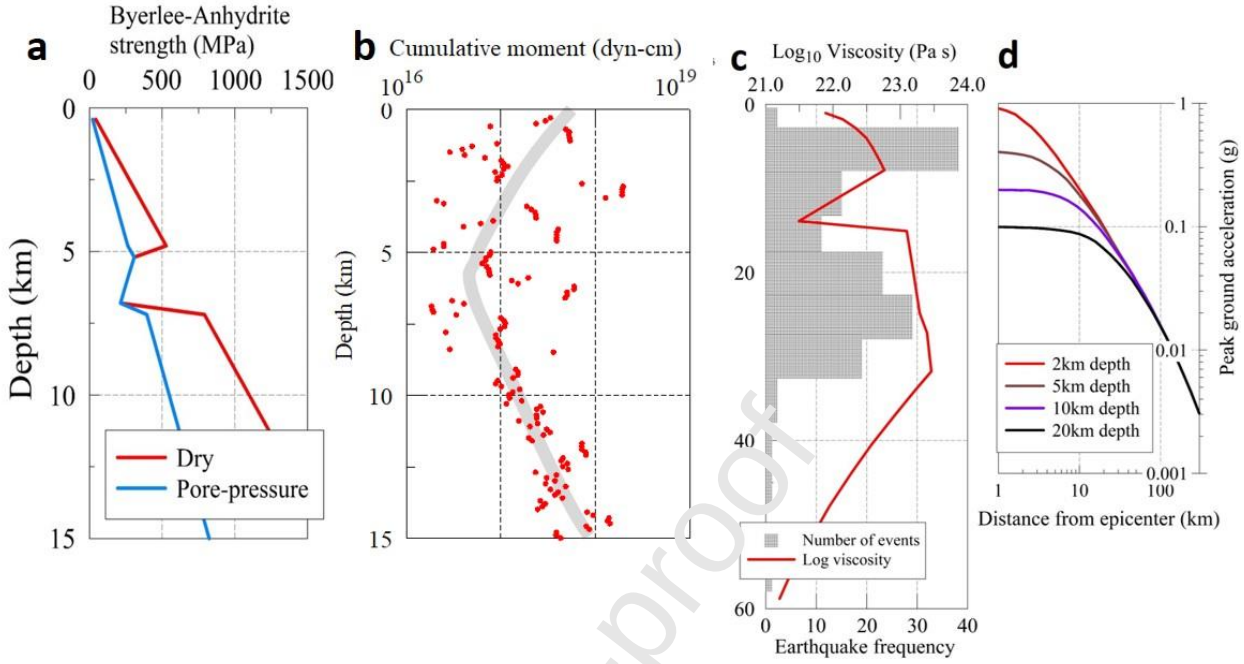

Fig. 8

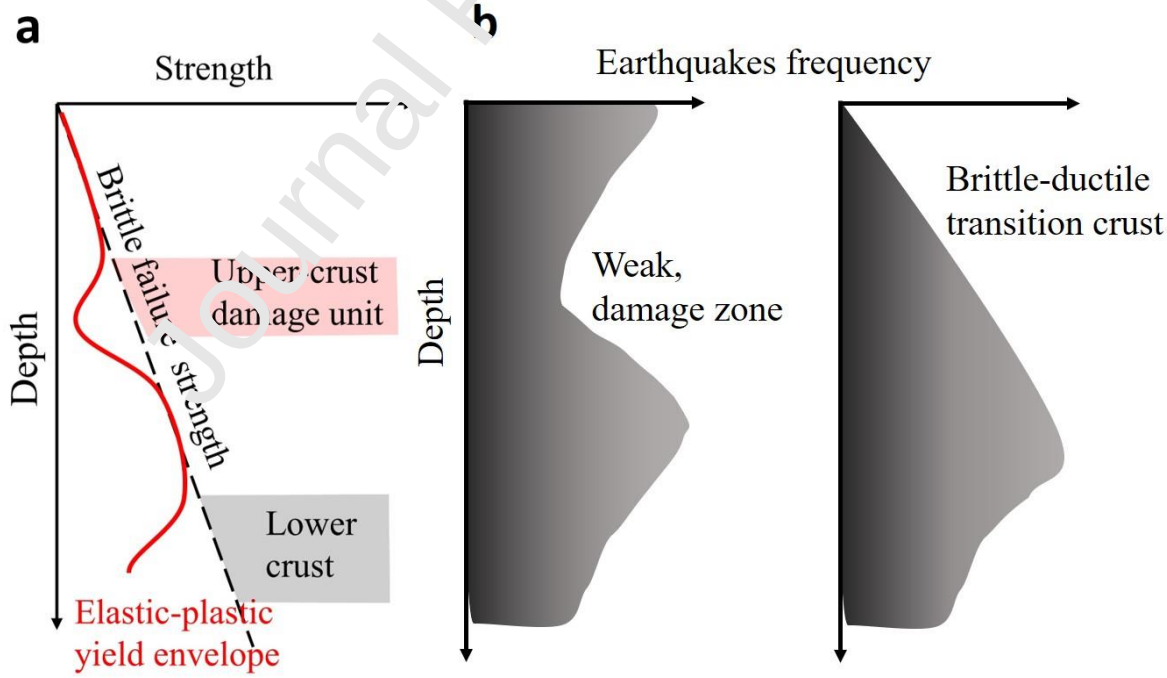

Fig. 9

Z. L. and Z. R. conceived of the presented idea. Z. L. and L. Z. developed the theory and performed the computations. H. Z. and F. H. verified the analytical methods. H. Z. encouraged Z.L. to investigate the faulting and supervised the findings of this work. Z. L. and Z. R. discussed the results and contributed to the final manuscript.

Declaration of interests

☐The authors declare that they have no known competing financial interests or personal relationships that could have appeared to influence the work reported in this paper.

☒The authors declare the following financial interests/personal relationships which may be considered as potential competing interests:

Zonghu Liao reports financial support was provided by Chinese Academy of Sciences. Zonghu Liao reports financial support was provided by National Key Research and Development Program of China. Zonghu Liao reports financial support was provided by ISF-NSFC Joint Scientific Research Program.

Highlights

- Damage from tectonic processes continuously weakens stratigraphic units to transform them into thick decollement zones;
- The depth distribution of seismic activity in the western Sichuan BasinBasin is controlled by a decollement zone composed of a damaged Triassic sequence;
- The existence of the 'damage stratigraphic' unit may pose a seismic hazard to the inhabitants of the Chengdu area.